Experimental Characterization of Separated Flows – A Review

Joseph Katz
Department of Mechanical Engineering
Johns Hopkins University
UNITED STATES

Katz@jhu.edu

ABSTRACT

The objective of this paper is to summarize the state of knowledge in experimental research focusing on separated flows. Owing to the breadth of this field, several specific cases have been selected as examples. Including are: (i) separated flows around blunt bodies and inclined bodies of revolution; (ii) the flow structure and turbulence associated with flow separation in turbulent boundary layers subjected to adverse pressure gradients (APG); and (iii) the flow structure around airfoils undergoing oscillatory pitching with amplitude high enough to cause dynamic stall. Samples of recently obtained velocity, vorticity, and pressure distributions of dynamic stall are also provided to demonstrate the complexity of this phenomenon, and the ability of PIV to resolve it. The discussion highlights the impact of recent advances in optical measurement techniques, including 2D-, stereo-, tomographic- and holographic-PIV on our abilities to characterize 3D flow structures in great detail. Time-resolved volumetric data can also be used for calculating the unsteady pressure field, enabling direct comparisons between flow structure and forces. Ongoing efforts to reduce the adverse effects of experimental errors using the Navier Stokes Equations are also mentioned.

1.0 INTRODUCTION

Experimental studies involving separated flows span a broad range of fields, too many to summarize in a single document. Hence, Chapter 2 of the present document focuses on studies where detailed understanding of the flow structure and turbulence are critical for understanding the processes involved. Included are boundary layer separation induced by adverse pressure gradients in turbulent boundary layer, the flow around blunt bodies, and the complex flow structure around airfoils subjected to pitching oscillations high enough to cause dynamic stall. Over the last twenty five years, measurement techniques available to the research community have evolved from point sensing using, e.g. hot wire anemometry (HWA) and laser doppler velocimetry (LDV), as well as qualitative visualization methods using, e.g. smoke or oil film on surfaces, which were prevalent until the mid 1990s, to imaging-based planar and volumetric measurement techniques, that are dominant these days. The hardware and software for performing 2D and 3D Particle Image Velocimetry (PIV) measurements are now commercially available from multiple companies, and several books [1] now provide comprehensive information about the procedures involved, from the imaging equipment, particle seeding, and data analysis procedures. Yet, implementation of PIV-based techniques requires careful preparations, e.g. image filtering in a noisy background, proper seeding, and assessment of data to determine whether it achieves the desired accuracy and resolution. For example, for three-dimensional time-resolved data, one can determine directly how well it

satisfies the equations of motion (continuity and momentum), and then develop methods to correct/interpolate it accordingly. Such techniques are subjects for ongoing research, as discussed in the conclusions.

2.0 SUMMARY OF PAST RESEARCH

2.1 3D Separated Flows Behind Blunt bodies and Inclined Bodies of Revolution

While considerable efforts have been invested in characterizing the flow and turbulence around inclined bodies of revolution, most of these experiments date back to the mid 1990s, and except for a few preliminary efforts to implement PIV (Fu et al. [2]), most of the measurements involved point sensors (Meier & Kreplin [3], Chesnakas & Simpson [4-6], Goody et al.[7] and Goody et al.[8], Wetzel & Simpson [9] and Wetzel et al. [10]), and surface flow visualizations (Han & Patel [11]). Recent related studies have been mostly based on various forms of numerical simulations. In contrast, there have been numerous PIV measurements around and behind blunt bodies with a broad range of geometries, from spheres (Brücker [12,13]), cylinders (Wiliamson [14], Kitzhofer et al. [15]), finite length cylinders (Provansal et al. [16]), etc.

In spite of the simple geometry, the flow structure behind e.g. spheres, is extremely complicated and Reynold number dependent. The wake structure behind spheres at low Reynolds numbers has been of particular interest owing to its impact on transport of particles in the ocean and the atmosphere. Considerable fraction of what is known on this wake has been derived from numerical simulations (e.g. Johnson & Patel [17]; Yun et al. [18]). Until recently, experiments aimed at characterizing the vortical structure of the wake behind sphere involved qualitative flow visualizations using dye or smoke (Sakamoto & Haniu [19], Leweke *et al.* [20]; Chrust et al. [21]). Prior to the availability of 3D measurement techniques, Brücker [12] used spatio-temporal reconstructions of the 3D wake based on time-resolved 2D PIV data in a transverse plane to characterize the 3D wake structure. Subsequently, 2D PIV and 3D particle tracking velocimetry (PTV) have been used by Doh et al. [22] and Jang & Lee[23]. Recent experiments involving volumetric 3D measurements using tomographic PIV were reported by Terra et al.[24], van Hout *et al.*[25], and Eshbal et al. [13]. The latter combined snapshots of tomographic PIV measurements with time-resolved planar PIV data to reconstruct the 3-D vortex shedding cycle in the wake of the sphere. They showed that the wake consisted of both a primary vortex chain shed from the sphere, and secondary vortices generated as the sphere's separating shear layer interacted with the counter-rotating longitudinal vortices extending downstream from the sphere.

2.2 Flow Separation by Adverse Pressure Gradient in Boundary Layers

A comprehensive review of the state of knowledge on boundary layer separation 30 years ago was provided by Simpson [26]. Boundary layer separation could be caused either by a sharp change in surface slope, e.g. a downstream facing step (e.g. Troutt et al. [27], Le et al. [28]), or by adverse pressure gradient (APG). The latter have been harder to characterize or model due sensitivity of the locations of separation and reattachment to small changes in pressure gradient (Simpson et al [29]). These studies showed that prior to separation, the turbulent boundary layer (TBL) decelerated and thickened until the separation point, where the wall shear stress vanished. The size of the separation bubble increased with the magnitude of pressure gradients (Alving & Fernholz [30]). Separated regions have been typically characterized by complex 3D flows even when the boundary conditions

were two dimensional, due, e.g., to effects of side walls in water/wind tunnels and diffusers (Malm et al. [31], Ashjaee & Johnston [32], Cherry et al. [33], Duquesne et al. [34]) or end effects (tip or hub) on lifting surfaces (Moss & Murdin [35], Broeren & Bragg [36] and Délery [37]).

In controlled experiments, the adverse pressure gradients were commonly created by installing a curved wall on the other side of the surface being investigated (Simpson et al. [38], Simpson et al. [29], Weiss et al. [39], Mohammed-Taifour & Weiss [40]). Another approach was to install a porous cylinder and apply suction (e.g. Dianat and Castro [41]) or adopt a variety of means to minimize the end effects (Thompson & Whitelaw [42]). Attempts to avoid 3D effects by studying axisymmetric flows (Dengel & Fernholz [43]) did not eliminate the circumferential nonuniformities (Délery [37]). Due to the fluctuations in the location of the separation, past measurements involving point sensors encountered flow in both directions at the same place, leading to introductions of parameters, e.g. intermittency, defining the fraction of time with forward flow (Simpson *et al.* [38], Simpson [44]). Other notable studies by Simpson's group attempting to develop scaling laws for the mean velocity profiles in separated flows have been Simpson [45] and Agarwal & Simpson [46]. It should be noted that intermittent reverse flow did not necessarily implies that the flow was separated, leading to questions how to determine whether separation actually occurred. The typically accepted condition defining separation in an unsteady flow has been a zero shear stress and a local streamwise velocity equal to the bulk velocity of the separated flow domain (Sears & Telionis [47]). Several other dynamical systems-based methods to define separation have been discussed e.g. in Surana et al. [48,49].

Considerable efforts have also been invested in characterizing the turbulence in separated flows. Simpson [44] classified the distributions of Reynolds stresses in 2D (mean sense) separated flows as a three-layer system, with a viscous low Reynolds stress region near the wall, an outer layer containing large scale turbulent structures that were prevalent outside of the separated region, and an overlap layer between them. As an inflection point developed in the APG region, the elevation of maximum turbulence production moved away from the wall, and turbulence transport was directed towards the wall (Krogstad & Skåre [50], Lee & Sung [51,52]). Quadrant analysis in the APG region upstream and within the separated region has also been the focus of several studies (Krogstad & Skåre [50], Song & Eaton [53], and Elyasi and Ghaemi [54]). In the inflected APG boundary layer, sweeps were dominant below the inflection point, and ejections above it.

A more recent hotwire and PIV based study involving a boundary layer with adverse pressure gradients followed by a flap (Couvier et al. [55]) provided a comprehensive picture on the distributions and causes for turbulence production and transport. Above the mean border of the separated zone, production of streamwise velocity fluctuations, in particular streamwise contraction, was the dominant contributor in the upstream part of the separated region. Further downstream, flapping of the shear layer became more important, and affected the production rate of the Reynolds shear stress and wall-normal velocity fluctuations.

Coherent structures have also been investigated both numerically and experimentally. The mechanisms and role of low speed streaks based mostly on DNS results was summarized by Lee & Sung [52]. The experimental data showed that large scale turbulent motions were dominated by breathing motions of the separated bubble, and shedding of spanwise vortices (Kiya & Sasaki [56], Cherry et al. [57], Hillier & Latour [57], Mohammed-Taifour & Weiss [40]). Proper Orthogonal Decomposition (POD), which has become a popular method for analysing and

interpreting PIV data, also showed that the first and most dominant POD mode was associated breathing motion (Mohammed-Taifour & Weiss [40]). The Strouhal number for this contraction and expansion of the separation was very low (*St*~0.01, Weiss *et al.* [39]), while values for the shear layer rollup and shedding were higher (St~0.35), in agreement DNS results by Na & Moin [58]. POD modes containing multiple singularities (foci and saddle points) for a plane parallel to a diffuser wall were discussed in Duquesne et al. [34]. Dominance of the first POD modes has also been observed in shock-induced separation (Humble et al. [59]), geometry-induced separation (Thacker et al. [60]), and adverse pressure gradient induced separation (Elyasi and Ghaemi [54]). The latter study involved applications of 2D and tomographic PIV to characterize the turbulence and 3D coherent structures associated with intermittent 3D separation in a predominantly 2D diffuser. Conditional sampling by matching the separation points prevented data smearing. Their Reynolds stresses peaked in the shear layer, consistent with previous studies (e.g. Song & Eaton [53,61]). Within the separation bubble the Reynolds stresses were low, also consistent with Simpson [26] and Cuvier et al. [55]. Since their APG-induced separation occurred on a flat surface (as opposed to a flap), Elyasi and Ghaemi [54] did not observe high initial streamwise velocity fluctuations, in contrast to Cuvier et al. [55], where the separation was sharp.

2.3 Separated Flows Behind Airfoils Undergoing Pitching Oscillations

The interest in the flow around airfoils undergoing oscillatory pitching, with and without concurrent heaving, has been driven in part by attempts to use them as a means of bio-inspired propulsion[62,63], and in part to investigate flutter and flow induced vibrations. Findings associated with heaving were summarized by [64]. Of the large body of literature on this topic, the discussion in this paper has been restricted mostly to studies of flow structure generated by oscillatory pitching. Classical qualitative flow visualizations of the vortices in the wake of a foil pitching at small amplitudes were introduced by Koochesfahani [65]. As summarized by McCroskey[66], as the oscillation amplitude increased, a phenomenon typically referred to as dynamic stall developed. On a 2D sinusoidally pitching airfoils, this phenomenon typically involved delay of the stall to higher incidence angles during an upstroke and consequently, a much higher lift and pitching moments relative to a steady flow. This process also involved formation and shedding of organized vortex structures on the suction side of the foil.

The works of Raffel et al.[67] and Wernert et al.[68] represented early efforts to use 2D PIV for characterizing the flow field on the suction side of a NACA 0012 airfoil under deep dynamic stall conditions. Instantaneous snapshots of data were used for observing the characteristic four phases of the stall process, namely attached flow, development of the dynamic stall vortex, post-stall vortex shedding, and reattachment of the boundary layer. During an upstroke, a stall vortex formed near the leading edge of the foil (will be referred to as LEV), grew to a large fraction of the suction side, and then migrated downstream. At maximum incidence, the large vortex was shed, and replaced by a series of co-rotating vortices originating from the leading edge along the shear layer defining the upper edge of the separated region. Concurrently, the backflow in the aft part of the foil entrained opposite-sign vorticity originating from pressure side from the near wake of the foil. The latter will be referred to as trailing edge vortex (TEV). During down stroke the enclosed circulating vortex/region reformed but its strength was smaller, and it migrated faster than that forming during the upstroke. Both trends were consistent with prior observations[69], which also showed that this vortex caused a considerable increase in lift. At low incidences this vortex stated migrating downstream and the forward part of the suction side flow reattached to the surface of the foil. In a follow-up paper, Wernert et al.[68] compared their findings to results of numerical

predictions showing reasonable agreement. Related considerations associated with phase averaging of highly unsteady data were discussed by Wernert and Favier[70]. Samples of dynamic stall obtained recently in our laboratory are presented in the next chapter.

A more recent PIV-based study involving combined plunging and pitching for a range of frequencies, amplitudes, and Reynolds numbers was performed by Fenercioglu and Cetiner [71]. They showed that the primary flow features, which were dominated by leading and trailing edge-generated vortices, was weakly dependent on the Reynolds number, but varied substantially with the Strouhal number. Another recent combined numerical-experimental study of a pitching foil was performed by Gharali and Johnson[72]. In addition to using a control volume analysis to estimate the lift and drag forces, they also utilized the phase-averaged PIV data to calculate the pressure distribution by integrating the Reynolds Equations assuming, a 2D flow, and Bernoulli's Equation for boundary conditions. The phase averaged data showed the formation of the LEV and TEV, and that both contributed to the lift force. The number of LEVs increased but the strength of each vortex decreased with reduced frequency, k=□fc/U, where f is the oscillation frequency, c is the chord-length, and U the freestream velocity. Increasing k also affected the phase delay between the angle of dynamic stall and that corresponding to maximum LEV circulation. Mackowski and Williamson[73] measured the thrust and efficiency as well as the vorticity distributions behind an airfoil undergoing oscillatory pitching. They also measured the unsteady forces on the foil and compared them to classical linear theories. Interestingly, while the linear theories overpredicted the thrust, the amplitude and phase of the unsteady component were predicted accurately. Hence, the authors concluded that that the thrust force generated by the pitching foil was insensitive to the vortical structure in its wake.

3.0 SAMPLES OD RECENT DATA OF DYNAMIC STALL

This section provides samples of velocity, vorticity and pressure distributions around an oscillating NACA 0012 foil, which were recorded recently in our laboratory, highlighting some of the above-mentioned processes associated with dynamic stall. The experiments have been performed in a refractive index-matched water tunnel, where the refractive index of the fluid, a concentrated aqueous solution of sodium iodide is matched with that of the acrylic foil. This setup has enabled detailed observations in multiple systems, from turbomachines (e.g. Chen et al. [74]) to rough wall boundary layers (Hong et al. [75,76]), etc. The foil chordlength is 50 mm, its span is 189 mm, the free stream velocity is 1.03 m/s, the Reynolds number is 4.5×10^4, the frequency is 2.77 Hz, resulting in a reduced frequency of 0.411, and the incidence angle varies between 5 to 20 degrees. The data has been recorded using stereo-PIV. The time-resolved 2048x2048 pixel images have been acquired at 1250 Hz, resulting in 463 realizations per cycle. In all cases, the vectors are diluted by for clarity. Owing to the refractive index matching, the measurements are performed on both sides of the foil simultaneously. Consistent with previous findings, the results show the delayed stall during the upstroke (Figure 1a), the formation and growth of an LEV near the maximum angle (Figures 1a & b), the substantially larger separated region during early phases of the downstroke (Figure 1c), the downstream migration of the vortex but its massive presence close to and at the end of the downstroke (Figures 1d and e), and the attachment of the flow to the leading edge during early phase of upstroke (Figure 1f)

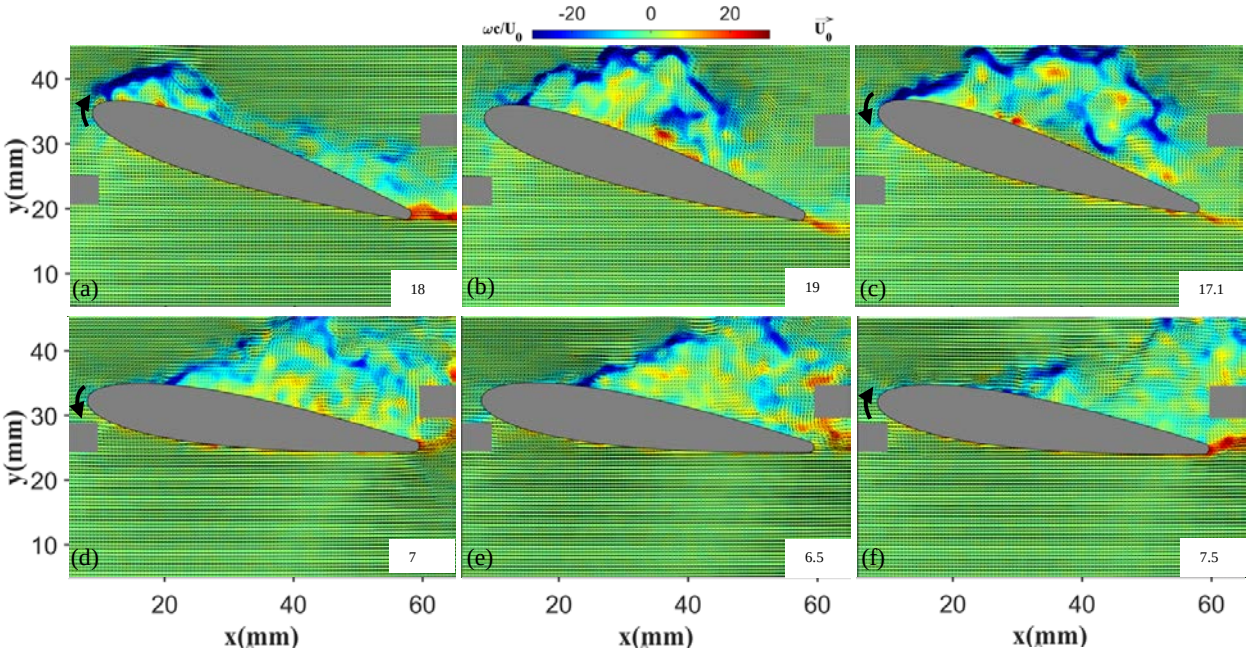

Figure 1: Sample instantaneous vorticity (color contours) and velocity (vectors) distributions around an oscillating airfoil showing the evolution of dynamic stall. The arrows near the leading edge show the direction of motion, and the inserts show the incidence angles in degrees. Vectors are diluted by 2:1 for clarity.

Assuming a predominantly 2D flow, the time-resolved data can be used for calculating the pressure distribution by integrating the material acceleration of the fluid. Details about the procedures for performing omni-directional integration, which is aimed at reducing the effect of experimental errors in acceleration, are provided in Liu and Katz [77,78] for 2D flows, and in Wang et al.[79] and Zhang et al. [80] for 3D flows. The latter parallel-line, omni-directional integration is performed using GPUs to accelerate the data processing rate. This procedure also includes means to evaluate the data quality based on the local magnitude of the curl of the pressure gradient (should be zero) and reduce the weight of specific integration paths with errors exceeding acceptable thresholds. The calculated pressure distribution corresponding to the data in Figure 1 is presented in Figure 2. Other recently introduced methods for instantaneous pressure calculations, which are based on solving the Pressure-Poisson Equation, are discussed and summarized by Van Oudheusden[81], and a comparative discussion about uncertainty is provided in Wang et al. [79] A recent effort to compare the performance of a series of different pressure measurement techniques is discussed van Gent et al. [82].

A direct comparison between Figures 1 and 2 show the impact of the growth and development of the vortices on the suction side on the load distribution, hence the aerodynamic pitching moment on the foil. In Figure 2a, the pressure minimum is located near the leading edge of the foil, but in Figure 2b, as the LEV grows and migrates, there are multiple pressure minima, with the largest one located in the aft part of the foil. The minimum near the

leading edge disappears as the downstroke begins and the vortex migrates to the aft part of the passage (Figure 2c). At the end of the downstroke, in Figure 2D, the pressure differences across the foil are small, and there is even a mild pressure minimum near the trailing edge of the pressure side, where the boundary layer thickens. In Figure 2e, the is a pressure minimum far from the surface, corresponding to a local presence of a large (counter-rotating) vortex. This intermittent structure does not persist once data are phase averaged. Finally, as the upstroke begins (Figure 2e), a near surface pressure minimum appears at the leading edge of the remnants of the separated region. This sequence, which provides samples from an on-going study, demonstrates the advantage in being able to characterize the causes, i.e. flow structure, and effects (pressure) as the flow around the oscillating foil evolves.

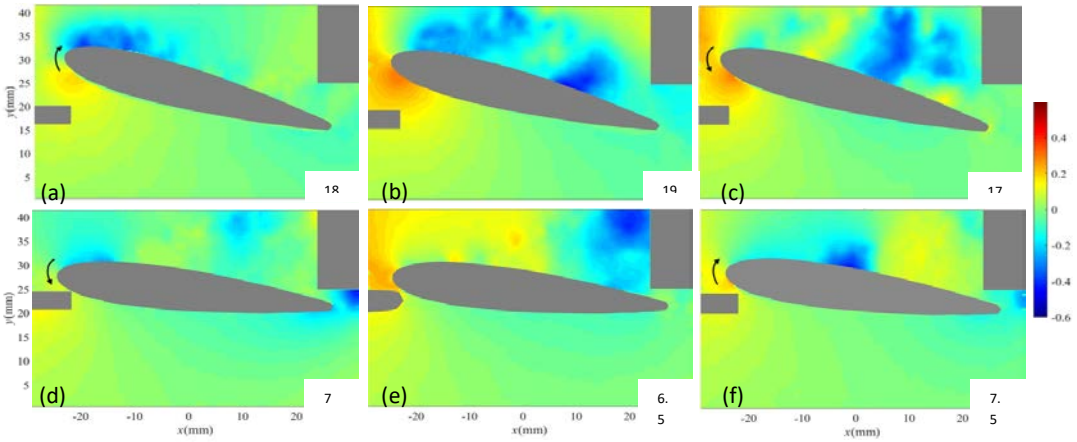

Figure 2: Instantaneous pressure (color contours) and velocity (vectors) distributions corresponding to the data presented in Figure 1.

4.0 CONCLUSIONS

The paper summarizes the state of knowledge in experimental research of separated flows around blunt bodies, in adverse pressure gradient turbulent boundary layers, and on airfoils undergoing oscillatory pitching with amplitude high enough to cause dynamic stall. Samples of recent velocity, vorticity, and pressure distributions of dynamic stall, which has been recorded recently in our laboratory, are also provided to demonstrate the complexity of this phenomenon. The discussions highlight the impact of recent advances in optical measurement techniques on our ability to characterize complex 3D flow structures in great detail. Before concluding this paper, one should mention that the development of advanced measurement techniques is an on-going process. Among the recently introduced procedures, notable ones that promise to have a great impact on characterization of separated flows are e.g.: (i) the introduction of the so-called “shake the box” Lagrangian particle tracking method for processing tomographic PIV images by Schanz et al.[83]; (ii) interpolation of tomographic PIV data by integrating solutions to the vorticity transport equation with the experimental data[84], and (iii) introduction of holographic tomography for measuring the 3D separated flow

around roughness elements embedded in the inner part of rough wall boundary layers at a micron resolution[85].

5.0 ACKNOWLEDGEMENT

Funding for the research performed in the JHU refractive index matched facility, including the equipment and analysis tools for recording the data and calculating the pressure distributions presented in chapter 3, has been provided by the Office of Naval Research. The research about dynamic stall was funded by the Airforce Office of Scientific Research.

6. REFERENCES

[1] Adrian, R. J. & Westerweel, J. *Particle image velocimetry*. 241-248 (Cambridge University Press, 2011).

[2] Fu, T. C., Shekarriz, A., Katz, J. & Huang, T. The flow structure in the lee of an inclined 6: 1 prolate spheroid. *Journal of Fluid Mechanics* **269**, 79-106 (1994).

[3] Meier, H. U. & Kreplin, H.-P. Experimental investigation of the boundary layer transition and separation on a body of revolution. *Zeitschrift fur Flugwissenschaften und Weltraumforschung* **4**, 65-71 (1980).

[4] Chesnakas, C. & Simpson, R. Full three-dimensional measurements of the cross-flow separation region of a 6: 1 prolate spheroid. *Experiments in Fluids* **17**, 68-74 (1994).

[5] Chesnakas, C. & Simpson, R. Measurements of the Turbulence Structure in the Vicinity of a 3-D Separation. *Journal of Fluids Engineering* **118**, 268-275 (1996).

[6] Chesnakas, C. J., Taylor, D. & Simpson, R. L. Detailed Investigation of the Three-Dimensional Separation About a 6:1 Prolate Spheroid. *AIAA Journal* **35**, 990-999 (1997).

[7] Goody, M., Simpson, R. & Engel, M. in *36th AIAA Aerospace Sciences Meeting and Exhibit.* 630.

[8] Goody, M. C., Simpson, R. L. & Chesnakas, C. J. Separated flow surface pressure fluctuations and pressure-velocity correlations on prolate spheroid. *AIAA journal* **38**, 266-274 (2000).

[9] Wetzel, T. G. & Simpson, R. L. Unsteady crossflow separation location measurements on a maneuvering 6 : 1 prolate spheroid. *Aiaa Journal* **36**, 2063-2071 (1998).

[10] Wetzel, T. G., Simpson, R. L. & Chesnakas, C. J. Measurement of Three-Dimensional Crossflow Separation. *AIAA Journal* **36**, 557-564 (1998).

[11] Han, T. & Patel, V. Flow separation on a spheroid at incidence. *J. Fluid Mechanics* **92**, 643-657 (1979).

[12] Brücker, C. Spatio-temporal reconstruction of vortex dynamics in axisymmetric wakes. *Journal of fluids and structures* **15**, 543-554 (2001).

[13] Eshbal, L., Rinsky, V., David, T., Greenblatt, D. & van Hout, R. Measurement of vortex shedding in the wake of a sphere at Re=465. *Journal of Fluid Mechanics* **870**, 290-315 (2019).

[14] Williamson, C. H. K. Vortex dynamics in the cylinder wake. *Ann. Rev. Fluid Mechanics* **28**, 477-539 (1996).

[15] Kitzhofer, J., Nonn, T. & Brucker, C. Generation and visualization of volumetric PIV data fields. *Experiments in Fluids* **51**, 1471-1492 (2011).

[16] Provansal, M., Schouveiler, L. & Leweke, T. From the double vortex street behind a cylinder to the wake of a sphere. *European Journal of Mechanics-B/Fluids* **23**, 65-80 (2004).

[17] Johnson, T. & Patel, V. Flow past a sphere up to a Reynolds number of 300. *Journal of Fluid Mechanics* **378**, 19-70 (1999).

[18] Yun, G., Kim, D. & Choi, H. Vortical structures behind a sphere at subcritical Reynolds numbers. *Physics of Fluids* **18**, 015102 (2006).

[19] Sakamoto, H. & Haniu, H. A study on vortex shedding from spheres in a uniform flow. *Journal of Fluids Engineering* **112**, 386-392 (1990).

[20] Leweke, T., Provansal, M., Ormieres, D. & Lebescond, R. Vortex dynamics in the wake of a sphere. *Physics of Fluids* **11**, S12-S12 (1999).

[21] Chrust, M., Goujon-Durand, S. & Wesfreid, J. Loss of a fixed plane of symmetry in the wake of a sphere. *Journal of Fluids and Structures* **41**, 51-56 (2013).

[22] Doh, D., Hwang, T. & Saga, T. 3D-PTV measurements of the wake of a sphere. *Measurement Science and Technology* **15**, 1059 (2004).

[23] Jang, Y. I. & Lee, S. J. PIV analysis of near-wake behind a sphere at a subcritical Reynolds number. *Experiments in Fluids* **44**, 905-914 (2008).

[24] Terra, W., Sciacchitano, A. & Scarano, F. Aerodynamic drag of a transiting sphere by large-scale tomographic-PIV. *Experiments in Fluids* **58**, 83 (2017).

[25] van Hout, R., Eisma, J., Elsinga, G. E. & Westerweel, J. Experimental study of the flow in the wake of a stationary sphere immersed in a turbulent boundary layer. *Physical Review Fluids* **3**, 024601 (2018).

[26] Simpson, R. L. Turbulent boundary-layer separation. *Ann. Rev. Fluid Mechanics* **21**, 205-232 (1989).

[27] Troutt, T., Scheelke, B. & Norman, T. Organized structures in a reattaching separated flow field. *Journal of Fluid Mechanics* **143**, 413-427 (1984).

[28] Le, H., Moin, P. & Kim, J. Direct numerical simulation of turbulent flow over a backward-facing step. *Journal of fluid mechanics* **330**, 349-374 (1997).

[29] Simpson, R. L., Chew, Y.-T. & Shivaprasad, B. The structure of a separating turbulent boundary layer. Part 1. Mean flow and Reynolds stresses. *Journal of Fluid Mechanics* **113**, 23-51 (1981).

[30] Alving, A. E. & Fernholz, H. Turbulence measurements around a mild separation bubble and downstream of reattachment. *Journal of Fluid Mechanics* **322**, 297-328 (1996).

[31] Malm, J., Schlatter, P. & Henningson, D. S. Coherent structures and dominant frequencies in a turbulent three-dimensional diffuser. *Journal of Fluid Mechanics* **699**, 320-351 (2012).

[32] Ashjaee, J. & Johnston, J. Straight-walled, two-dimensional diffusers—transitory stall and peak pressure recovery. *Journal of Fluids Engineering* **102**, 275-282 (1980).

[33] Cherry, E. M., Elkins, C. J. & Eaton, J. K. Geometric sensitivity of three-dimensional separated flows. *International Journal of Heat and Fluid Flow* **29**, 803-811 (2008).

[34] Duquesne, P., Maciel, Y. & Deschênes, C. Unsteady flow separation in a turbine diffuser. *Experiments in Fluids* **56**, 156 (2015).

[35] Moss, G. & Murdin, P. *Two dimensional Low-speed Tunnel Tests on the NACA 0012 Section Including Measurements Made During Pitching Oscillations at the Stall*. (Royal Aircraft Establishment, 1968).

[36] Broeren, A. P. & Bragg, M. B. Spanwise variation in the unsteady stalling flowfields of two-dimensional airfoil models. *AIAA journal* **39**, 1641-1651 (2001).

[37] Délery, J. *Three-dimensional separated flow topology: critical points, separation lines and vortical structures*. (John Wiley & Sons, 2013).

[38] Simpson, R. L., Strickland, J. & Barr, P. Features of a separating turbulent boundary layer in the vicinity of separation. *Journal of Fluid Mechanics* **79**, 553-594 (1977).

[39] Weiss, J., Mohammed-Taifour, A. & Schwaab, Q. in *53rd AIAA Aerospace Sciences Meeting*. 1289.

[40] Mohammed-Taifour, A. & Weiss, J. Unsteadiness in a large turbulent separation bubble. *Journal of Fluid Mechanics* **799**, 383-412 (2016).

[41] Dianat, M. & Castro, I. P. Turbulence in a separated boundary layer. *J. fluid mechanics* **226**, 91-123 (1991).

[42] Thompson, B. & Whitelaw, J. Characteristics of a trailing-edge flow with turbulent boundary-layer separation. *Journal of Fluid Mechanics* **157**, 305-326 (1985).

[43] Dengel, P. & Fernholz, H. An experimental investigation of an incompressible turbulent boundary layer in the vicinity of separation. *Journal of Fluid Mechanics* **212**, 615-636 (1990).

[44] Simpson, R. L. Aspects of turbulent boundary-layer separation. *Prog. in Aerospace Sci.* **32**, 457-521 (1996).

[45] Simpson, R. L. A model for the backflow mean velocity profile. *AIAA journal* **21**, 142-143 (1983).

[46] Agarwal, N. K. & Simpson, R. L. Backflow structure of steady and unsteady separating turbulent boundary

layers. *AIAA journal* **28**, 1764-1771 (1990).

[47] Sears, W. R. & Telionis, D. P. Boundary-Layer Separation in Unsteady Flow. *SIAM Journal on Applied Mathematics* **28**, 215-235 (1975).

[48] Surana, A., Grunberg, O. & Haller, G. Exact theory of three-dimensional flow separation. Part 1. Steady separation. *Journal of fluid mechanics* **564**, 57-103 (2006).

[49] Surana, A., Jacobs, G. B., Grunberg, O. & Haller, G. An exact theory of three-dimensional fixed separation in unsteady flows. *Physics of Fluids* **20**, 107101 (2008).

[50] Krogstad, P. Å. & Skåre, P. E. Influence of a strong adverse pressure gradient on the turbulent structure in a boundary layer. *Physics of Fluids* **7**, 2014-2024 (1995).

[51] Lee, J.-H. & Sung, H. J. Effects of an adverse pressure gradient on a turbulent boundary layer. *International Journal of Heat and Fluid Flow* **29**, 568-578 (2008).

[52] Lee, J.-H. & Sung, H. J. Structures in turbulent boundary layers subjected to adverse pressure gradients. *Journal of Fluid Mechanics* **639**, 101-131 (2009).

[53] Song, S. & Eaton, J. The effects of wall roughness on the separated flow over a smoothly contoured ramp. *Experiments in fluids* **33**, 38-46 (2002).

[54] Elyasi, M. & Ghaemi, S. Experimental investigation of coherent structures of a three-dimensional separated turbulent boundary layer. *Journal of Fluid Mechanics* **859**, 1-32 (2018).

[55] Cuvier, C., Foucaut, J. M., Braud, C. & Stanislas, M. Characterisation of a high Reynolds number boundary layer subject to pressure gradient and separation. *Journal of Turbulence* **15**, 473-515 (2014).

[56] Kiya, M. & Sasaki, K. Structure of a turbulent separation bubble. *J. Fluid Mechanics* **137**, 83-113 (1983).

[57] Cherry, N., Hillier, R. & Latour, M. Unsteady measurements in a separated and reattaching flow. *Journal of Fluid Mechanics* **144**, 13-46 (1984).

[58] Na, Y. & Moin, P. Direct numerical simulation of a separated turbulent boundary layer. *Journal of Fluid Mechanics* **374**, 379-405 (2002).

[59] Humble, R., Scarano, F. & Van Oudheusden, B. Unsteady aspects of an incident shock wave/turbulent boundary layer interaction. *Journal of fluid mechanics* **635**, 47-74 (2009).

[60] Thacker, A., Aubrun, S., Leroy, A. & Devinant, P. Experimental characterization of flow unsteadiness in the centerline plane of an Ahmed body rear slant. *Experiments in fluids* **54**, 1479 (2013).

[61] Song, S. & Eaton, J. K. Flow structures of a separating, reattaching, and recovering boundary layer for a

large range of Reynolds number. *Experiments in fluids* **36**, 642-653 (2004).

[62] Platzer, M. F., Jones, K. D., Young, J. & Lai, J. C. S. Flapping-wing aerodynamics: Progress and challenges. *Aiaa Journal* **46**, 2136-2149 (2008).

[63] Mccroskey, W. J. Unsteady Airfoils. *Annual Review of Fluid Mechanics* **14**, 285-311 (1982).

[64] Lai, J. C. S. & Platzer, M. F. Jet characteristics of a plunging airfoil. *Aiaa Journal* **37**, 1529-1537 (1999).

[65] Koochesfahani, M. M. Vortical Patterns in the Wake of an Oscillating Airfoil. *Aiaa J.* **27**, 1200-1205 (1989).

[66] McCroskey, W. J. The Phenomenon of Dynamic Stall., (1981).

[67] Raffel, M., Kompenhans, J. & Wernert, P. Investigation of the unsteady flow velocity field above an airfoil pitching under deep dynamic stall conditions. *Experiments in Fluids* **19**, 103-111 (1995).

[68] Wernert, P., Geissler, W., Raffel, M. & Kompenhans, J. Experimental and numerical investigations of dynamic stall on a pitching airfoil. *AIAA journal* **34**, 982-989 (1996).

[69] Leishman, J. G. Dynamic Stall Experiments on the Naca-23012 Aerofoil. *Exp. in Fluids* **9**, 49-58 (1990).

[70] Wernert, P. & Favier, D. Considerations about the phase averaging method with application to ELDV and PIV measurements over pitching airfoils. *Experiments in Fluids* **27**, 473-483 (1999).

[71] Fenercioglu, I. & Cetiner, O. Categorization of flow structures around a pitching and plunging airfoil. *Journal of Fluids and Structures* **31**, 92-102 (2012).

[72] Gharali, K. & Johnson, D. A. PIV-based load investigation in dynamic stall for different reduced frequencies. *Experiments in Fluids* **55**, 1803 (2014).

[73] Mackowski, A. & Williamson, C. Direct measurement of thrust and efficiency of an airfoil undergoing pure pitching. *Journal of Fluid Mechanics* **765**, 524-543 (2015).

[74] Chen, H., Li, Y., Tan, D. & Katz, J. Visualizations of Flow Structures in the Rotor Passage of an Axial Compressor at the Onset of Stall. *Journal of Turbomachinery* **139**, 041008-041008-041014 (2017).

[75] Hong, J., Katz, J., Meneveau, C. & Schultz, M. P. Coherent structures and associated subgrid-scale energy transfer in a rough-wall turbulent channel flow. *Journal of Fluid Mechanics* **712**, 92-128 (2012).

[76] Hong, J., Katz, J. & Schultz, M. P. Near-wall turbulence statistics and flow structures over three-dimensional roughness in a turbulent channel flow. *Journal of Fluid Mechanics* **667**, 1-37 (2011).

[77] Liu, X. & Katz, J. Instantaneous pressure and material acceleration measurements using a four-exposure

PIV system. *Experiments in Fluids* **41**, 227 (2006).

[78] Liu, X. & Katz, J. Vortex-corner interactions in a cavity shear layer elucidated by time-resolved measurements of the pressure field. *Journal of Fluid Mechanics* **728**, 417-457 (2013).

[79] Wang, J., Zhang, C. & Katz, J. GPU-based, parallel-line, omni-directional integration of measured pressure gradient field to obtain the 3D pressure distribution. *Experiments in Fluids* **60** (2019).

[80] Zhang, C., Wang, J., Blake, W. & Katz, J. Deformation of a compliant wall in a turbulent channel flow. *Journal of Fluid Mechanics* **823**, 345-390 (2017).

[81] Van Oudheusden, B. PIV-based pressure measurement. *Measurement Science & Tech.* **24**, 032001 (2013).

[82] van Gent, P. L., Michaelis, D., van Oudheusden, B. W., Weiss, P. E., de Kat, R., Laskari, A., Jeon, Y. J., David, L., Schanz, D., Huhn, F., Gesemann, S., Novara, M., McPhaden, C., Neeteson, N. J., Rival, D. E., Schneiders, J. F. G. & Schrijer, F. F. J. Comparative assessment of pressure field reconstructions from particle image velocimetry measurements and Lagrangian particle tracking. Experiments in Fluids 58 (2017).

[83] Schanz, D., Gesemann, S. & Schroder, A. Shake-The-Box: Lagrangian particle tracking at high particle image densities. Experiments in Fluids 57 (2016).

[84] Schneiders, J. F. G. & Scarano, F. Dense velocity reconstruction from tomographic PTV with material derivatives. Experiments in Fluids 57 (2016).

[85] Gao, J. & Katz, J. Self-calibrated microscopic dual-view tomographic holography for 3D flow measurements. Optics Express 26, 16708-16725 (2018).